

C039

Seismic Imaging by Frequency-domain Double-beamforming Full-waveform Inversion

R. Brossier* (University of Joseph Fourier) & P. Roux (University of Joseph Fourier)

SUMMARY

Full waveform inversion is a promising imaging technology to delineate high resolution images of the subsurface, but suffers from intrinsic non-linearities that require adequate preconditioning. In this study, we investigate a frequency-domain double-beamforming full waveform inversion method (DBF-FWI). Objective is to take benefit of the array information through a double-beamforming (double slant-stack) to project the standard point-to-point data to the angles domain on the source and receiver arrays. The DBF procedure allows to improve significantly the signal-to-noise ratio of the DBF data, and the angles domain allows to select arrivals of interest without any time-domain mute. We illustrate on a synthetic example how the combination of DBF and FWI allows to define a new hierarchical level based on angles, which control image resolution, in order to precondition and improve the robustness of FWI.

Introduction

Quantitative seismic imaging of subsurface parameters is one of the main challenge for oil and gas reservoir characterisation. Full-waveform inversion (FWI) allows to derive high-resolution quantitative models of the subsurface through the exploitation of the full information content of the data (Taran-tola, 1984). When applied in the frequency domain, computationally efficient FWI algorithms can be designed by limiting the inversion to a few judiciously chosen discrete frequencies (Sirgue and Pratt, 2004). However, FWI remains an ill-posed and highly non-linear inverse problem that is sensitive to noise, inaccuracies of the starting model, lack of low frequencies in conventional seismic data and definition of multiparameter classes. In order to limit these effects, several hierarchical approaches have been proposed to mitigate the non-linearities of the inverse problem : low to high frequency reconstruction (Bunks et al., 1995; Sirgue and Pratt, 2004), data preconditioning by exponential decay (Brossier et al., 2009b; Brenders et al., 2009), data component and parameter selection (Sears et al., 2008; Brossier et al., 2009a).

Classically, FWI is written as a global summation over the acquisition survey of single source/ single receiver couples. Despite some recent developments tried to use simultaneous source with source-stacking and phase-encoding strategies for 3D FWI (Ben Hadj Ali et al., 2009; Herrmann et al., 2009; Krebs et al., 2009), these approaches do not take benefit of array information and try to mimic the results of point-to-point (PTP) data. However, with the common usage of dense seismic acquisition arrays, one can take benefit of array information to process the seismic data. Techniques such as time-delay beamforming (slant-stack) can therefore be used to identify and select arrivals while improving the signal-to-noise ratio. Under the source/receiver reciprocity principle, the beamforming can be applied in cascade on both the source and the receiver (sub-)arrays, giving a double-beamforming (DBF) technique (see Rost and Thomas, 2002, for a review).

In this study, we combine the DBF and the acoustic frequency-domain FWI methods. The objective is to make use of the benefits of the DBF advantages, namely the improved signal-to-noise ratio and the arrivals identification/ selection. This method provides a new preconditioning strategy for FWI, based on emission and reception angles on the acquisition array, which control image resolution and should improve the robustness of FWI.

Theory

FWI recalls : FWI is an optimization problem that is generally recast as a local non-linear least-squares problem. In the frequency domain and for a single frequency, the objective function is :

$$\mathcal{E} = \sum_{k=1}^{ns} \frac{1}{2} \Delta \mathbf{d}_k^t \overline{\Delta \mathbf{d}_k}, \quad (1)$$

where $\Delta \mathbf{d}_k = \mathbf{d}_{obs_k} - \mathbf{d}_{calc_k}$ is the data misfit vector: the difference between the observed data vector \mathbf{d}_{obs_k} and the modelled data vector \mathbf{d}_{calc_k} for the source k . Superscripts t and $^-$ denote the transpose and conjugate operators, respectively. The vector \mathbf{d}_{calc_k} is obtained by applying a sampling operator \mathbf{S} to the full incident wavefield \mathbf{u}_k that results from the forward-problem system $\mathbf{A}\mathbf{u}_k = \mathbf{s}_k$. The matrix \mathbf{A} is the forward-problem matrix that discretizes the Helmholtz equation and which depends non-linearly on the wave-speed model \mathbf{m} . The vector \mathbf{s}_k is the source term that represents the acoustic source excitation. ns is the number of source in the acquisition

The gradient of the cost function can be derived from the adjoint-state formalism (Plessix, 2006):

$$\mathcal{G}_{m_i} = - \sum_{k=1}^{ns} \Re \left\{ \mathbf{u}_k^t \frac{\partial \mathbf{A}^t}{\partial m_i} \overline{\lambda}_k \right\}$$

where \Re denotes the real part of a complex number. The gradient can be seen as a product (zero-lag correlation in time), between the incident wavefield $\mathbf{u}_k = \mathbf{A}^{-1}\mathbf{s}_k$ from the source vector \mathbf{s}_k , and the adjoint wavefield $\overline{\lambda}_k = \mathbf{A}^{-1}\mathbf{S}^t\overline{\Delta \mathbf{d}_k}$, using residuals at receiver positions as a composite source. The radiation pattern of the diffraction by the model parameter m_i is denoted by the sparse matrix $\partial \mathbf{A} / \partial m_i$.

Double beamforming : Double beamforming is a two-step procedure applied on the PTP data in the $(t, \mathbf{x}_s, \mathbf{x}_r)$ domain, where t is time, and \mathbf{x}_s and \mathbf{x}_r are the source and receiver positions. Assuming that the velocity profile is known on the arrays, beamforming (slant-stack) is applied in cascade on source and receiver sub-arrays, projecting the data to the $(t, \mathbf{x}_{s0}, \mathbf{x}_{r0}, \phi, \theta)$ domain, where ϕ and θ are the emission and reception angles on the source and receiver sub-arrays, respectively. Note that DBF is applied on sub-arrays whose size should be optimally close to the first Fresnel zone's size (Iturbe et al., 2009). Finally, a data-selection is applied in the $(t, \mathbf{x}_{s0}, \mathbf{x}_{r0}, \phi, \theta)$ domain, in order to choose angles that maximize energy of desired arrivals.

After DBF processing and selection, if we consider one DBF of index k related to the pair of angles (ϕ_k, θ_k) for the sub-arrays centres \mathbf{x}_{r0_k} and \mathbf{x}_{s0_k} , the frequency-domain expression of the DBF data is given by:

$$d_k = \sum_{r=1}^{n_{rec}} \alpha_{k_r} \sum_{s=1}^{n_{src}} \beta_{k_s} d_{r,s}, \quad (2)$$

where the summations are performed over the limited numbers of receivers n_{rec} and sources n_{src} . The PTP frequency-domain data $d_{r,s}$ is generated by the source s and measured at the receiver r , and α_{k_r} and β_{k_s} are the receiver and source phase-shifts associated to the DBF k .

DBF-FWI: The DBF-FWI cost function can be simply written as:

$$\mathcal{C} = \sum_{k=1}^{ndbf} \frac{1}{2} \Delta d_k^t \overline{\Delta d}_k, \quad (3)$$

where the summation is applied on the number of the DBF ($ndbf$) in this case. Each beamforming k is calculated from the source and receiver sub-array centres $(\mathbf{x}_{s0_k}, \mathbf{x}_{r0_k})$ and the number of sub-array elements n_{src} and n_{rec} , through the associated phase shifts (α_k, β_k) .

After some substitutions, we end up with the expression of the DBF-FWI gradient :

$$\begin{aligned} \mathcal{G}_{m_i} &= - \sum_{k=1}^{ndbf} \Re \left\{ \sum_{r=1}^{n_{rec}} \alpha_{k_r} \sum_{s=1}^{n_{src}} \beta_{k_s} \mathbf{s}_s^t \mathbf{A}^{-1} \frac{\partial \mathbf{A}^t}{\partial m_i} \mathbf{A}^{-1} \mathbf{S}^t \mathbf{s}_r \overline{\Delta d}_k \right\} \\ &= - \sum_{k=1}^{ndbf} \Re \left\{ \sum_{s=1}^{n_{src}} \beta_{k_s} \mathbf{s}_s^t \mathbf{A}^{-1} \frac{\partial \mathbf{A}^t}{\partial m_i} \sum_{r=1}^{n_{rec}} \mathbf{A}^{-1} \mathbf{S}^t \mathbf{s}_r \alpha_{k_r} \overline{\Delta d}_k \right\}, \end{aligned} \quad (4)$$

where \mathbf{s}_s and \mathbf{s}_r are the impulse source terms located at the source s and receiver r , respectively. As for the classical gradient of Eq. (2), this gradient expression shows the product of three terms:

1. the wavefield $\sum_{s=1}^{n_{src}} \beta_{k_s} \mathbf{s}_s^t \mathbf{A}^{-1}$, which represents the incident wavefield from a plane wave located on the source array at position \mathbf{x}_{s0_k} with an incident angle θ_{s_k} (computed from phase-shifts β_{k_s}).
2. the sparse matrix $\partial \mathbf{A}^t / \partial m_i$, which represents the diffraction sensitivity of parameter m_i .
3. the wavefield $\sum_{r=1}^{n_{rec}} \mathbf{A}^{-1} \mathbf{s}_r \alpha_{k_r} \overline{\Delta d}_k$, which represents the adjoint wavefield from a plane wave located on the receiver array at position \mathbf{x}_{r0_k} , with an incident angle θ_{r_k} (computed with phase-shifts α_{k_r}), and with an amplitude term $\overline{\Delta d}_k$. This term represents the back-propagation of the residual, as for classical FWI.

Sensitivity Kernels

We first focus on the effects of DBF on sensitivity kernels. Figure 1 illustrates the real part of the PTP and DBF kernels in a homogeneous infinite wave-speed model (1500 m/s) at the frequency of 6.8 Hz. Source and receiver are located at positions $(x=500 \text{ m}, z=1500 \text{ m})$ and $(x=8500 \text{ m}, z=1500 \text{ m})$, respectively. The classical PTP kernel is the classical wavepath, which exhibits the first Fresnel zone and also secondary fringes associated with the interference pattern in the monochromatic approach. The DBF kernel is built by considering 0° incident plane waves on the source and receiver arrays (incidence parallel to survey). Beamforming is applied to 11 elements on each sub-array, which corresponds to 1000 m of antennae. The DBF kernel clearly shows a single sensitivity zone that cannot be related to the first Fresnel zone. This sensitivity zone is built by the constructive summation of each PTP phase-shifted

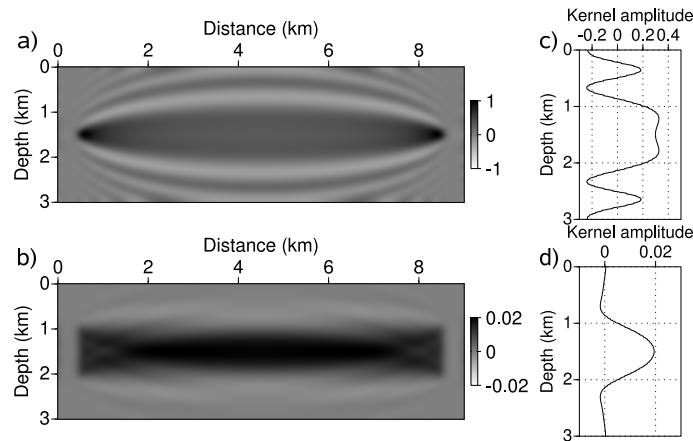


Figure 1 wave-speed sensitivity kernels for (a) PTP acquisition and (b) DBF. Panels (c) and (d) are cross-sections for the kernels at position $x = 4,500$ m for (a) and (b), respectively.

kernel of the source and receiver sub-arrays, and it can be related to plane-wave Fraunhofer diffraction. The secondary fringes of the PTP kernels are destructively summed during the DBF summation, which naturally means that the sensitivity kernel is weaker in the zones where the finite-width plane wave does not propagate. In summary, the DBF-FWI kernel highlights the spatial focusing of kernel sensitivity only where the finite-width plane wave travels, in contrary to the classical FWI kernel, which spreads the sensitivity over a wider area that is associated with the diffraction-based point-spread function of a point-like source-receiver pair.

Realistic application : Offshore Valhall

A imaging application focuses on the acoustic synthetic Valhall model (Figure 2-(a)). An acquisition system composed of 315 sources and 315 receivers, each 50 meters, mimics an Ocean Bottom Cable survey. The free-surface is considered in this study meaning that surface-multiple are present in the data. The Figure 3-(a) shows an example of a shot-gather for a source located at position $x=8100$ m. Inversion is performed for 5 frequencies from 2 Hz to 7 Hz, starting from a smooth starting model (Figure 2-(b)). DBF processing is performed for sub-arrays composed of 21 elements on sources and receivers (1000 meters antennae), and for one central element each 10 elements of the acquisition geometry. Note that DBF could be applied on a finer sub-sample of the survey to improve quality of the results, because this under-sampling of the data leads to a dramatic reduction of the data volume used in FWI.

In order to illustrate how the angles selection on sub-arrays in DBF controls the arrivals taken into account, DBF-FWI is performed in three steps for the angles ranges : $[\pm 60^\circ, \pm 30^\circ]$, $[\pm 60^\circ, \pm 15^\circ]$ and $[\pm 60^\circ, 0^\circ]$. As it is illustrated on Figure 3, this angle selection allows to choose the arrivals involved in the FWI process without any time-domain windowing despite the frequency-domain formulation. The first DBF range ($[\pm 60^\circ, \pm 30^\circ]$) allows to select the first arrival and very wide angle refractions. The range $[\pm 30^\circ, \pm 15^\circ]$ allows to add pre-critical reflections associated to intermediate diffraction angles, while the final $[\pm 15^\circ, 0^\circ]$ range concerns the short offset reflections associated to small diffraction angles. The resolution power associated to these angle ranges is illustrated in the reconstructed models (Figure 2), which show how, for the same frequency range considered, the selection on angles on sub-arrays is linked to the diffraction angles and therefore control the resolution of the imaged structures. That DBF approach provides an additional multi-scale reconstruction based on angles, which acts as a preconditioner for FWI to mitigate some nonlinearities.

Conclusion

This study presents a combined DBF and frequency-domain FWI scheme for subsurface quantitative imaging. The main advantages of this DBF-FWI scheme are linked to the improved SNR of the data thanks to the double summation of the DBF process, which can be particularly useful for low frequency inversion. The method allows also to select the arrivals based on angles that defines a new hierarchical level in order to precondition FWI to mitigate the non-linearities effects, and that could be useful for target-oriented imaging to focus on arrivals of interest.

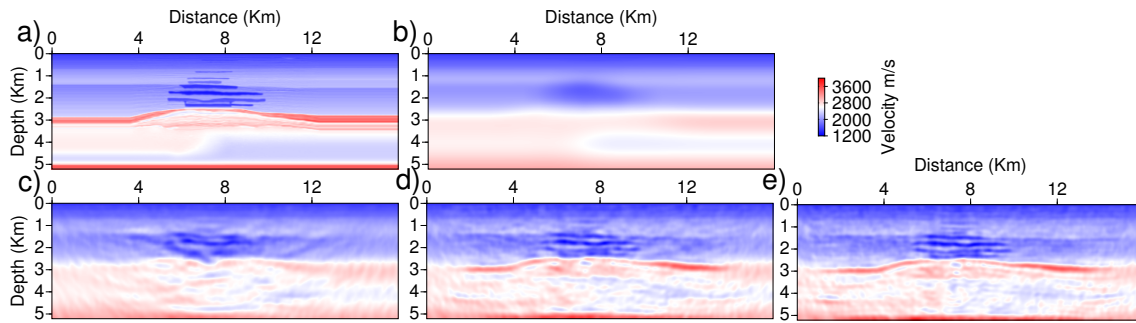


Figure 2 (a) True and (b) initial models of the Valhall application. Reconstructed model after inversion of angle ranges (c) $[\pm 60^\circ, \pm 30^\circ]$, (d) $[\pm 60^\circ, \pm 15^\circ]$ and (e) $[\pm 60^\circ, 0^\circ]$.

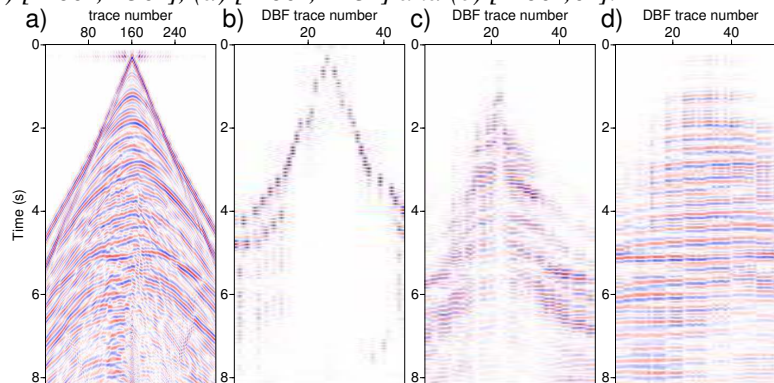


Figure 3 (a) Initial shot gather (source at $x=8100\text{m}$), associated DBF data for the angle ranges (b) $[\pm 60^\circ, \pm 30^\circ]$, (c) $[\pm 30^\circ, \pm 15^\circ]$ and (d) $[\pm 15^\circ, 0^\circ]$. All data are plotted with AGC.

Acknowledgements

This work was partially performed using HPC resources of the Géoazur laboratory cluster (Université Nice Sophia-Antipolis), the LGIT laboratory (Université Joseph Fourier, Grenoble) and from GENCI-[CCRT/CINES/IDRIS] (Grant 2010-046091). R. Brossier is supported by Réseaux de Transport d'Electricité under project 08CUF1954. This study was partially supported by the SEISCOPE consortium (<http://seiscope.oca.eu>), which is sponsored by BP, CGG-Veritas, ENI, EXXON-Mobil, SHELL, STATOIL and TOTAL.

References

- Ben Hadj Ali, H., Operto, S. and Virieux, J. [2009] Three-dimensional frequency-domain full waveform inversion with phase encoding. *79th Annual SEG Conference & Exhibition, Houston, SEG*, 2288–2292.
- Brenders, A., Pratt, R. and Charles, S. [2009] Waveform tomography of 2-d seismic data in the canadian foothills - data preconditioning by exponential time-damping. *Expanded Abstracts, EAGE*, U041.
- Brossier, R., Operto, S. and Virieux, J. [2009a] Two-dimensional seismic imaging of the Valhall model from synthetic OBC data by frequency-domain elastic full-waveform inversion. *SEG Technical Program Expanded Abstracts, Houston*, **28**(1), 2293–2297.
- Brossier, R., Operto, S. and Virieux, J. [2009b] Seismic imaging of complex onshore structures by 2D elastic frequency-domain full-waveform inversion. *Geophysics*, **74**(6), WCC63–WCC76, doi:10.1190/1.3215771.
- Bunks, C., Salek, F.M., Zaleski, S. and Chavent, G. [1995] Multiscale seismic waveform inversion. *Geophysics*, **60**(5), 1457–1473.
- Herrmann, F.J., Erlangga, Y.A. and Lin, T.T.Y. [2009] Compressive simultaneous full-waveform simulation. *Geophysics*, **74**(4), A35–A40.
- Iturbe, I., Roux, P., Virieux, J. and Nicolas, B. [2009] Travel-time sensitivity kernels vs diffraction pattern obtained through double beamforming in shallow water. *J. Acoust.Soc. Am*, **126**(2), 713–720.
- Krebs, J. et al. [2009] Fast full-wavefield seismic inversion using encoded sources. *Geophysics*, **74**(6), WCC105–WCC116.
- Plessix, R.E. [2006] A review of the adjoint-state method for computing the gradient of a functional with geophysical applications. *Geophysical Journal International*, **167**(2), 495–503.
- Rost, S. and Thomas, C. [2002] Array seismology: methods and applications. *Reviews of Geophysics*, **40**(3), 1008, doi:10.1029/2000RG000100.
- Sears, T., Singh, S. and Barton, P. [2008] Elastic full waveform inversion of multi-component OBC seismic data. *Geophysical Prospecting*, **56**(6), 843–862.
- Sirgue, L. and Pratt, R.G. [2004] Efficient waveform inversion and imaging : a strategy for selecting temporal frequencies. *Geophysics*, **69**(1), 231–248.
- Tarantola, A. [1984] Inversion of seismic reflection data in the acoustic approximation. *Geophysics*, **49**(8), 1259–1266.